Numerical Simulation of Transonic Wind Tunnel DNW-HST including Slotted Walls at Supersonic Mach Numbers

Stefan Melber-Wilkending
German Aerospace Center (DLR)
Lilienthalplatz 7, 38108 Braunschweig
GERMANY
Stefan.Melber@dlr.de

Frenk Wubben
German-Dutch Wind Tunnels (DNW)
Anthony Fokkerweg 2, 1059 CM Amsterdam
THE NETHERLANDS
Frenk.Wubben @dnw.aero

Roy Gebbink
German-Dutch Wind Tunnels (DNW)
Anthony Fokkerweg 2, 1059 CM Amsterdam
THE NETHERLANDS
Roy.Gebbink @dnw.aero

ABSTRACT

To improve wind tunnel simulation capabilities and accuracy, an advanced numerical toolchain of the slotted wall DNW-HST transonic wind tunnel is created. Whereas earlier CFD simulations of the slotted wall tunnel environment have aided in the increased understanding of experimental results at subsonic flow conditions, this paper now demonstrates the numerical simulation capability for the transonic and low-supersonic flow regime.

The development of the numerical toolchain is presented via a discussion of the simulation strategy and an example of a wall- and support influence assessment for a basic delta wing configuration at Mach number 1.05 in both free flight and the in-tunnel environment. The developed toolchain forms the basis for further optimizations of the DNW-HST regarding flow quality, power consumption, Mach number range and some non-linearities that take place e.g. with bigger models in the test section.

1.0 INTRODUCTION

Most of today's wind tunnel facilities used for development work on industrial airplane configurations or for research of basic flow phenomena are designed long time ago using either empirical methods or idealized lumped-parameter models of the tunnel circuit. Already in case of subsonic flow and even more for trans- and supersonic flow the empirical models reach their frontier of applicability in forecasting complex effects in wind tunnels. To overcome this, the design is often supported by smaller prototype tunnels to examine the flow aspects of the complete wind tunnel or parts of it.

Over the last 40 years, numerical methods for the simulation of flow fields were developed and used in the research community dealing with initially simple configurations (e.g. isolated wings) and later used in the

industrial design work (already more or less complete aircraft). In parallel, numerical methods became more and more refined regarding e.g. turbulence modelling and robustness for real complex configurations.

Because wind tunnels still play an important role in the design of aircraft, the question arises if numerical simulation can help in planning, understanding and evaluating wind tunnel tests; in particular for developing detailed insights in wall- and support interference effects. Not only the experiment itself can be treated by numerical simulation, but also the redesign and improvement of an existing tunnel or even the complete design of a new wind tunnel.

This paper will focus on transonic wind tunnels because of its aerodynamic complexity which is the result of the non-linear interaction of sub- and supersonic flow and the resulting change in flow behaviour between both types of flow even in small distances in the flow field. A complex system of couplings in the flow field take place in transonic wind tunnel e.g. plenum pressure and its influence on the test section Mach number. Because of such non-linear couplings, redesign of isolated tunnel components or e.g. optimization of settings of variable elements is not easy only based on theory and measurements.

A fruitful cooperation between the German Aerospace Center (DLR) and the German-Dutch Wind Tunnels (DNW) was initiated many years ago to closely couple the experimental and the numerical simulation capabilities from both partners. The already existing experience in subsonic wind tunnel analysis and design is now extended to transonic and supersonic wind tunnel flows by numerical simulation of the DNW's High-speed tunnel (HST) with its slotted test section.

Various efforts to simulate subsonic wind tunnel flow by means of numerical methods have already been undertaken by many collaborators in the past. A large number of publications on this topic are summarized in [14]. For the current paper, the focus is specifically on transonic wind tunnels with slotted or perforated walls. A first publication in this specific field can be found from Glazkov et al [6] treating with the numerical simulation of a single slot of the European Transonic Wind tunnel (ETW) in subsonic flow at Mach number 0.8. Still treating numerical simulation of subsonic flow in an automotive wind tunnel with completely resolving slotted wind tunnel geometry can be found in [15].

In the time range from 2012 to 2018 several efforts were undertaken to investigate wall interferences in slotted (and some perforated) test sections by using porous wall boundary conditions for the slots instead of resolving the slots geometrically [7,8,18]. Especially Hantrais-Gervois et al [9] implement a porous boundary condition for the simulation of the Onera S2MA wind tunnel. The authors performed a detailed analysis based on actual measurements of the slot flow at a variation of the pressure difference between test section and plenum as basis for such a boundary condition for subsonic flow. However, this kind of boundary condition assumes well-defined or spatially constant flow conditions inside the slots. These assumptions may be valid for empty test section cases or with relatively small models compared to the tunnel cross section. But as soon the models get bigger with increasing wall interference these assumptions are not valid anymore; especially in transonic flow regime.

For the DNW-HST Maseland et al [13] used fully slot-resolving simulations at subsonic Mach numbers to investigate wall interference effects. Wubben et al [21] again treats the DNW-HST with numerical methods to investigate support and wall interference with slot resolving simulations at high subsonic Mach numbers of 0.78. For the ETW Kursakov et al [11] demonstrated simulations of the slotted test section in 2017 for subsonic flow. As a follow-up, Koenig et al [10] used Lattice Boltzmann methods to investigate the flow in the ETW slotted test section with a high degree of details of the geometry at a Mach number of 0.85. For American wind tunnels, still at subsonic flow of Mach numbers between 0.7 and 0.85 Rivers et al [16] have demonstrated numerical simulations of a very detailed geometry based on laser scans of the national transonic facility (NTF) located at the NASA Langley Research Center (LaRC) resolving the flow in the slots.

First results treating trans- and supersonic flow in slotted test sections again by Rivers et al [17] uses numerical methods for full slot resolving simulations of the wind tunnel NTF and the NASA Ames 11ft transonic wind tunnel. In that paper simulations of the test section with the CRM model at subsonic Mach numbers are shown. For supersonic Mach number of Ma = 1.2 only the empty test section was investigated. Finally, Chwalowski et al [1] shows fully resolved slotted test section simulations of the NASA Langley Research Center Transonic Dynamics Tunnel (TDT) at Mach numbers from 0.5 up to 1.1 for the empty test section and for a high subsonic Mach number including a fighter aircraft.

The next logical step is the numerical simulation of a wind tunnel, here on the example of DNW-HST, at transonic and supersonic Mach numbers with an aircraft model inside the test section and for a range of angles of attack. Not only the aircraft model should be considered but also all tunnel features like support system, side wall compensations for support, as well as the full treatment of the slots, the plenum, the re-entry area and the diffusor. All is to resemble the real DNW-HST and to get all the effects of the flow field.

The aim of this paper is to increase the understanding of the wind tunnel experiment at trans- and supersonic Mach numbers and to demonstrate the use of numerical simulation as a capability for an optimization of the DNW-HST regarding flow quality, power consumption, Mach number range and some non-linearities that take place e.g. with bigger models in the test section. To this end, a number of aircraft and tunnel configurations were investigated with the numerical simulation for analysis of the complete flow field.

This paper will show the development of the simulation strategy by discussing the simulation strategies and demonstrate its advantages on the example of transonic wall- and support influence in the DNW-HST. This example is part of an ongoing effort at DNW-HST to reduce the various experimental uncertainty in pursuit of "free flow" test results. The current supersonic assessments are a follow-up on the earlier validation and verification activities on the adequacy of the correction procedures for wind tunnel interference effects like support and wall interference at high subsonic Mach numbers [5,22].

Numerical simulations are conducted for a basic delta wing configuration (WEAG TA-15) in both the free flight and the in-wind tunnel environment at identical reference flow conditions. Because of the sensitivity of the flow in the transonic flow regime the Mach number 1.05 was chosen as the main condition. In both environments the model without and with four different supports was simulated to assess model support and wall interference effects. The benefit of using numerical simulation is that it offers the possibility to provide consistent results for both environments, which is not possible in an experimental approach.

Further on some numerical and experimental results will be presented regarding the influence on the flow field of slotted and perforated walls at transonic Mach numbers.

2.0 GEOMETRIES & NUMERICAL SIMULATION

The geometry of the DNW-HST wind tunnel and the WEAG TA-15 delta wing configuration are introduced in this chapter. The numerical domain and the mesh generation with the SOLAR mesh generator is described. Finally, the flow solver DLR-TAU is introduced.

2.1 Wind tunnel & WEAG model geometry

2.1.1 Wind Tunnel DNW-HST

The numerically modelled test facility is the DNW High-Speed Tunnel (HST) located in Amsterdam, the Netherlands. The DNW-HST is a pressurized continuous-flow wind tunnel suited for aircraft configuration testing at subsonic and transonic speeds. The shell structure of the wind tunnel allows the facility to be pressurized or evacuated, enabling testing at constant Reynolds numbers (figure 1). The air in the circuit is

driven by an axial compressor which comprises of several rows of rotor vanes with adjustable blade pitch which allow the Mach number to be kept constant within ±0.002 during operation. The attainable range in stagnation pressure is from 25 to 390 kPa and the operational stagnation temperature ranges between 275 and 320 K.

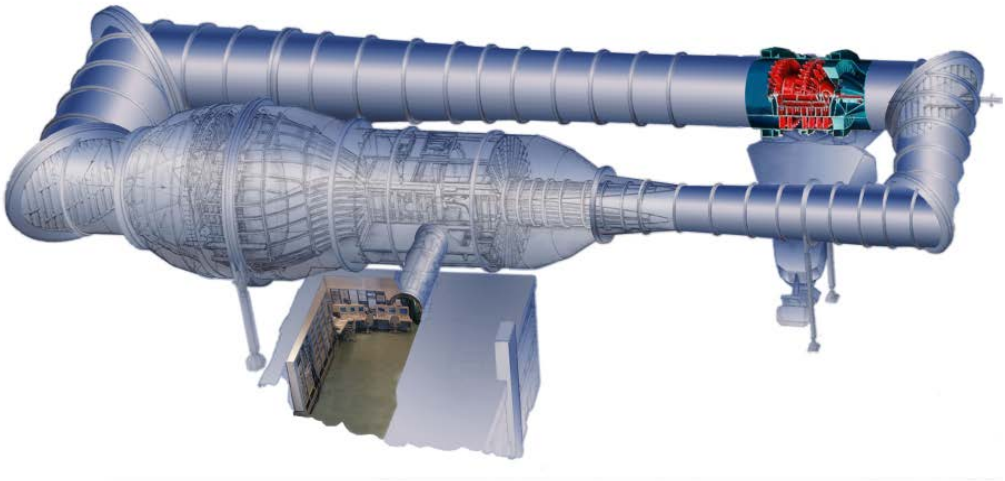

Figure 1: Overall layout of wind tunnel DNW-HST

An adjustable nozzle is followed by a rectangular test section with solid side walls and movable slotted upper and lower walls with openness ratio of 12%. The slots have a rectangular cross section of 50 mm x 6 mm. The upper and lower walls can be adjusted to obtain a test section height of 1.60 m or 1.80 m. The width of the test section is 2.0 m. For the work of this paper, the 2.0 m x 1.8 m test section is used. The test section is surrounded by a plenum chamber to accommodate ventilation of the air through the slotted walls. Downstream in the test section a permanently installed vertical strut provides interfacing for several types of model support systems. The test section is calibrated for Mach numbers between 0.2 and 1.3.

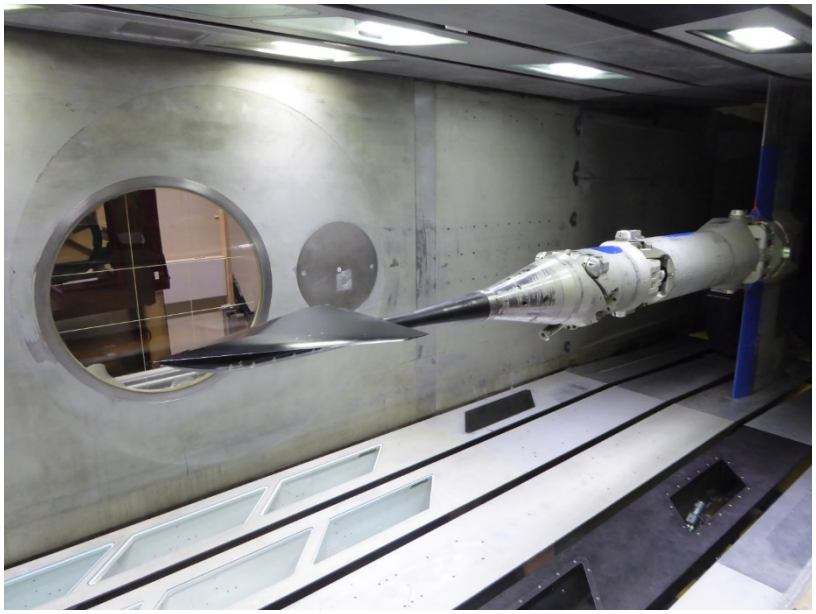

Figure 2: WEAG model in the DNW-HST slotted test section

2.1.2 WEAG model configuration

As an example test article, the WEAG TA-15 model is used in the slotted test section, see figure 2. The WEAG model is a simple delta wing configuration with a streamlined body mounted underneath. The delta wing has an overall length of 600 mm, a leading edge sweep angle of 65˚ and a reference wing area of 0.164 m^2. The main geometrical data are summarized in Table 1.

In figure 3 the movement of the support system for angle of attack 0 and 40 degrees is shown. To change to positive angle of attack, the horizontal part of the support is moving down while the front conical part including the sting pitches up. The movement is such that the model reference point is kept on the tunnel centerline. The latter is to minimize the wall influence on the model and to keep the model in the middle of the Schlieren window during testing.

Table 1: Geometric and simulation reference data of WEAG model

Wing Area S	0.164 m^2
Span B	0.4756 m
X-coord at root L	0.6 m
X-coord at wing tip c_t	0.09 m
Sweep of LE Λ_{LE}	65 deg
Reference density ρ	0.413 kg/m^3
Reference temperature T	236 K
Reference pressure p	28 kPa
Reference Mach number Ma	1.05

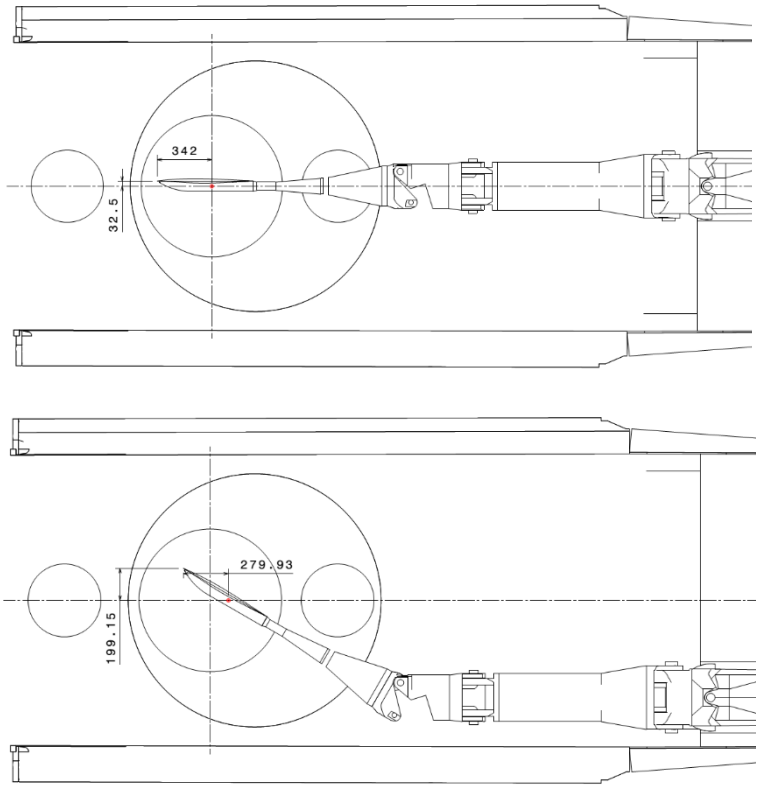

Figure 3: WEAG model at angle of attack 0 and 40º and resulting position of the support

2.1.3 Support / Sting Configurations

A total of five sting-support configurations are treated, in which for comparison the free flying aircraft without any support is included, see figure 4. In the subsequent, support means the combination of the main support boom and the sting between model and support boom. The main boom remains unaltered, but the stings are changed amongst the four configurations. For the free flying case, there is no support at all.

The “standard” type support from figure 4 is considered as the starting point. This combination of sting and support is normally used for models of size of the WEAG model in the DNW-HST. It permits a wide angle of attack range and keep at the same time the model reference point on the tunnel axis. The minimum cross section of the sting is limited by the aerodynamic forces during testing. Directly behind the fuselage a cross section reduction of the sting is visible. Derived from that the so called “slim” sting is envisaged. It uses a constant cross section sting as long and close as possible up to the alpha hinge. Again, starting from the standard type, an upstream shifting of the cone, which changes the cross section from the sting, to the alpha hinge is the “short” one. An even more upstream shifting of this cone creates the “very short” sting. The two latter configurations and even the slim sting will of course not be used in real wind tunnel tests but they are used in the numerical simulations for demonstrating the resulting effects.

No support / Free flying

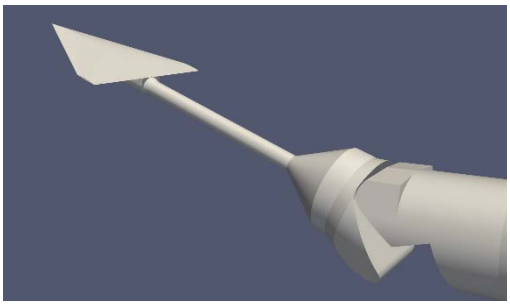

Slim sting

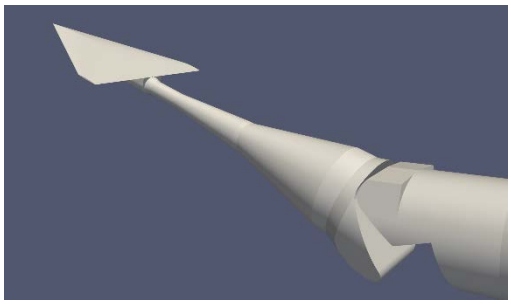

Standard sting

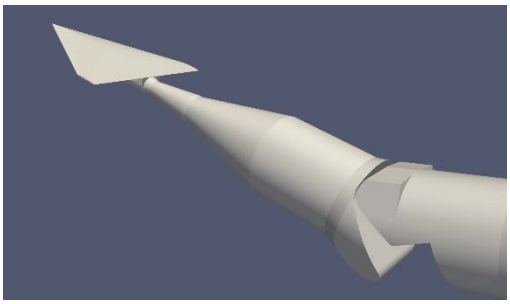

Short sting

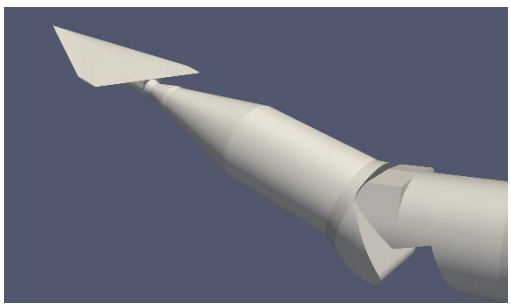

Very short sting

Figure 4: Five model support geometries

2.2 Computational Domain and Simulation Strategy

In figure 5 the complete domain treated by the numerical simulation is shown. The simulation starts at the end of the flow straighteners and screens package in the settling chamber of the wind tunnel. There the boundary conditions on the walls are well known because there is only a thin boundary layer (simplified as no boundary layer in CFD) and at the same time the screens create a constant total pressure and total temperature distribution over the cross section which can be used for the inflow boundary condition as a given value.

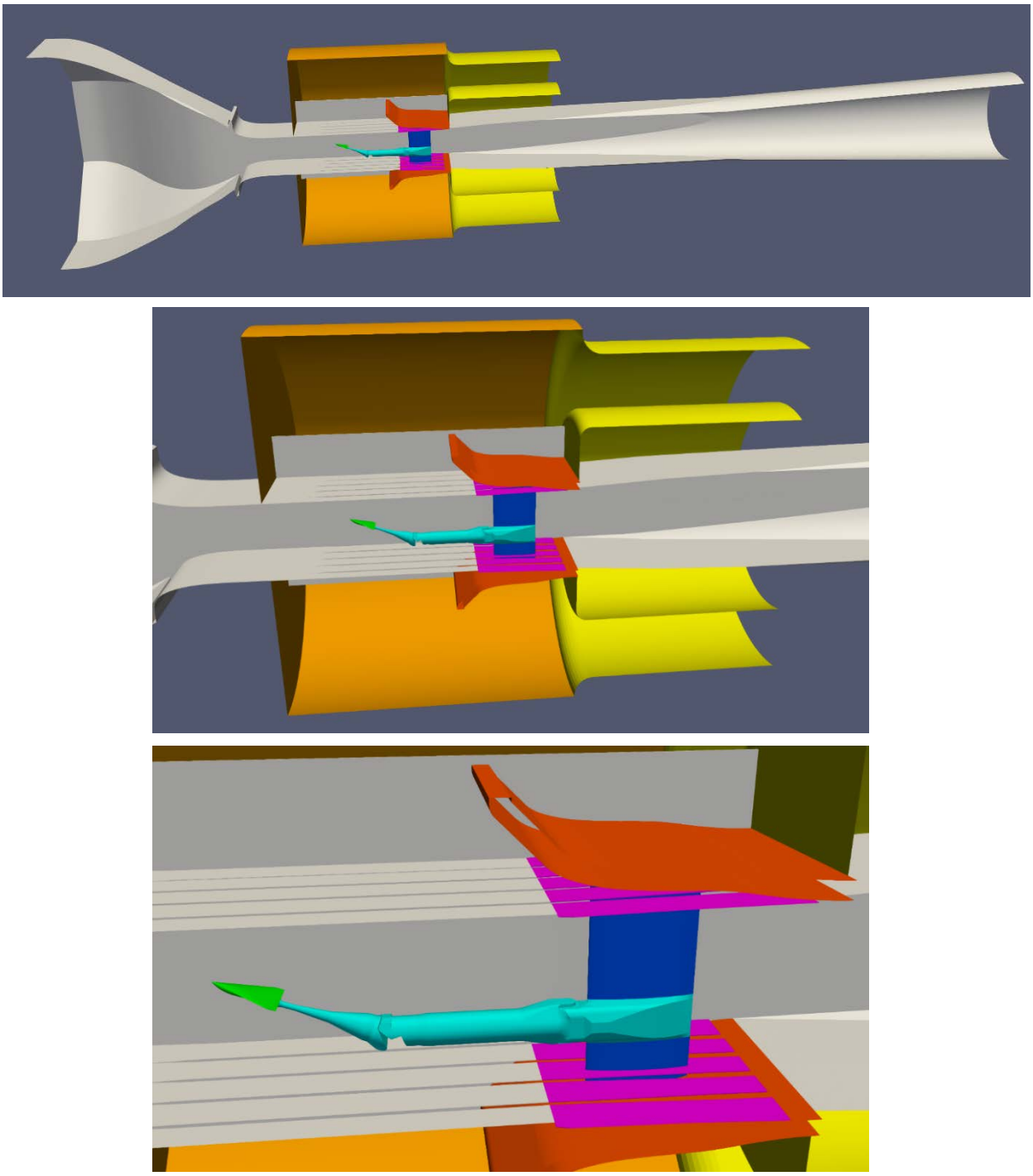

Figure 5: Domain of the numerical simulation.

The first feature within the computational domain is the subsonic contraction (most left grey part in figure 5) where the tunnel cross section gets reduced more and more. After that an interface plate on the lower and upper wall is visible. Here a supersonic Laval nozzle is flexibly connected with the subsonic contraction allowing for a controlled change of the cross section of the Laval nozzle throat area. The area ratio from the throat to the cross section of the test section defines the Mach number in the (empty) test section. So for each Mach number, a fixed throat area in combination with a Laval nozzle contour is given and kept constant during a polar.

The test section divergent upper and lower walls are slotted (12% opening ratio) which adds some extra complexity to the numerical simulation. As already discussed, a fully resolved simulation of such slots is needed. This means there is no need for any kind of extra boundary condition but does imply much more complexity in the mesh generation and of course much more mesh points have an effect on the overall simulation time.

Looking from the test section "behind" these slots the plenum is visible (depicted as the orange region in figure 5). The modelled plenum has the correct size but is simplified compared to the real tunnel. Various electrical and mechanical installations are omitted from the computational geometry. It was reasoned that such objects will mainly lead to dissipation on the flow. Hence, for the numerical simulation, the mesh in the plenum region is treated coarse to add up some numerical dissipation and create the same effect.

Downstream of the plenum chamber, a yellow part is visible in figure 5. This part of the computational domain does not exist in the real tunnel. Instead, it is used optionally in the numerical simulation to steer the plenum pressure directly by a fixed pressure boundary condition located on the right end of the figure. In real tunnel operation, the compressor affects the test section back pressure through the second and first turning vane and the diffusor. At the end of the test section a purple part (called slats extensions in DNW-HST, sometimes re-entry flaps) is installed which can be rotated like a flap. Below the slats extensions the so-called flaps are installed (red in figure 5) which can be moved vertically up and down. The trailing edge of the slat extensions forms a horizontal slot which mainly couples the pressure in the start of the diffusor with the plenum. The slats and flaps are not moved during a test polar but for different model sizes and Mach number combinations the settings can be changed.

If the test section static pressure is low enough compared to the settling chamber pressure, it results in sonic flow in the throat of the Laval nozzle and supersonic flow downstream. The static pressure in the test section can be changed by changing the back pressure with the compressor via the diffusor and plenum chamber. The target static pressure in the plenum is close but not equal to the static pressure of the flow in the test section. If the plenum pressure is lowered more outflow through the slots occurs which leads to an increase in the effective cross-sectional area and hence an increase in Mach number in the ventilated test section. The other way around a higher plenum pressure leads to a Mach number reduction in the test section.

In normal operation of the wind tunnel, a terminating shock occurs near the trailing edge of the slat extensions and consequently converts the supersonic flow to subsonic flow. When reducing the static pressure in the diffusor by increasing the compressor fan blade angle, this terminating shock might move downstream into the diffusor and will create increased losses in the flow. So, the setting of the slat extensions and flaps have to be optimized to fix the terminating shock at the slat trailing edge for all supersonic wind tunnel conditions. This is a delicate optimization, as the main compressor can only influence the plenum pressure via the subsonic wakes behind the slat trailing edges. In case the terminating shock would move too far into the diffusor, the plenum pressure cannot be regulated anymore by the compressor because there is no subsonic wake anymore to "communicate" through.

In the numerical simulation all this coupled flow is treated up to the end of the diffusor. This means the outlet static pressure of the diffusor can be used to finally change the plenum pressure like in real tunnel operation. However, because of the complex flow field of the tunnel mixing sub- and supersonic flow, a numerical

regulation of the plenum pressure is very sensitive and takes many iterations (and thereby computational costs). Therefore, this more complex way of regulating the plenum pressure is only used e.g. for the optimization of the slat extensions and flaps positions. But in case the assessments are more related to e.g. the test section and the model interaction, the plenum pressure can directly be set by the plenum pressure boundary condition to the static pressure of the test section (yellow part). In that case, the outlet pressure of the diffusor is kept constant at a value low enough to create supersonic flow in the test section.

The elements left in the description of figure 5 are the sword (dark blue part), which in real tunnel extents into the plenum but cut with the flaps in the numerical simulation. The support (light blue) moves up and down along the sword (in real tunnel the sword moves up and down and with it the support) to keep the model at centerline during changing of the model angle of attack. Because of the different geometry for different angles of attack, a new mesh is needed for each single angle of attack. Finally, the model (green in figure 4) is installed upstream of the support.

The complete domain described above is treated by the numerical simulation. Therefore, a mesh for discretizing that domain has to be created. Details on that topic will be discussed in the next chapter.

2.3 Mesh generation (SOLAR)

The hybrid unstructured grid for the resolution of the computational domain was generated with the SOLAR grid generator. SOLAR was developed jointly by ARA, QinetiQ, BAE Systems, and Airbus [2,12]. It discretizes surfaces with a mixed-element highly quad-dominant grid. To improve the overall element quality triangular elements are employed locally. The near-field advancing-layer grid for the resolution of the boundary layer is hexahedra-dominant, with some triangle-based prismatic layer stacks. Pyramidal elements are used to achieve a conformal interface between the near-field advancing-layer grid and the far-field advancing-front grid based on tetrahedra.

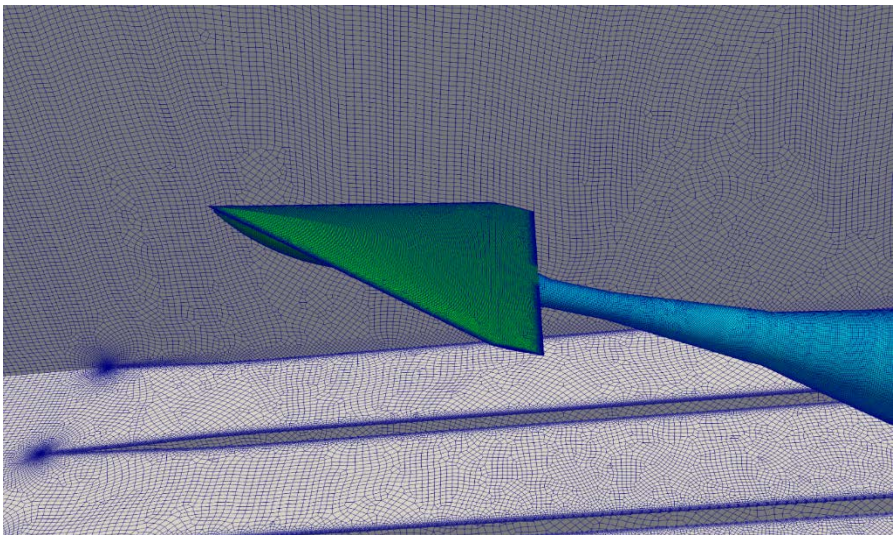

Figure 6: Surface mesh of test section and WEAG model.

SOLAR is used in a semi-automated mode, where the geometry of the configuration is subdivided in several zones of either lifting surfaces, bodies or the elements of the wind tunnel. Based on this subdivision, a set of surface- and volume sources is automatically distributed for each component. The aim is first to establish preferably structured areas with hexahedral elements, for example at the leading and trailing edges of the wing. Second, in highly curved regions like wing leading edges, anisotropy is used to reduce the overall number of points. The amount of triangular surface elements is typically in the order of 0.1% - 0.4% of the total surface

elements. In figure 6, as an example, the surface grid of the WEAG geometry, the support and parts of the test section is shown.

The DNW-HST wind tunnel configuration features areas of special challenges for the grid generation. These are mainly the slots because of the significant change in mesh size. Further on the support which is modelled in most details gives some challenging problems for the mesh generation. The free flight configurations use the same mesh size distributions as the in tunnel meshes but with removal of all tunnel components. All surfaces are modeled as viscous walls in the flow solver and resolved by about 40 – 50 layers of hexahedra in the mesh. Finally, despite the complexity of the numerical domain, an overall high grid quality was reached with about 160 million points for each configuration.

During the start of the project, grid sensitivity studies have been carried out with variation of the grid resolution e.g. in the flow field around the aircraft (especially in regions of shocks), slots in the tunnel walls or details of the aircraft itself like leading edge resolution. Finally, from that study maximum element sizes at different regions of the mesh are derived keeping the overall point number in mind.

2.4 Flow Solver (DLR TAU)

The numerical flow simulations presented in this paper use the finite-volume solver TAU developed by DLR [19], which solves the compressible flow equations on unstructured meshes with different cell types (e.g. hexahedra, tetrahedra or prisms). A wide range of RANS turbulence models and even scale-resolving capabilities using either wall-resolved LES or hybrid RANS/LES methods, the latter based on variants of Detached-Eddy Simulation (DES), are available in TAU.

In this paper the Spalart-Allmaras (SA) turbulence model [20] was used mainly because of its well-known stability even in complex flow fields. During the development of the simulation strategy tests with the more sophisticated Reynolds stress model RSM [3,4] where carried out with success. However, the differences to the less computational SA turbulence model were relatively small even in regions with stronger viscous effects like shock boundary layer interactions.

In terms of temporal discretization, an implicit 2nd-order backward scheme using dual-time stepping with non-linear sub-iterations, which are solved to a given convergence level by an implicit LU-SGS scheme were used. All simulations are steady state because there are only few local areas with time dependent variations in the flow field like vortex cores in the delta wing or some small flow separations on the sword. Time accurate simulations were also carried out for more detailed investigations regarding time response of the tunnel regulation system and to speed-up simulations which regulate the plenum pressure only by back pressure of the diffusor.

For the spatial discretization, a 2nd-order upwind AUSMDV scheme was used, on the coarse multigrid grids the flux is discretized by a Van Leer scheme. To speed up the convergence to steady was driven by a 2v multigrid scheme.

The initialization scheme of the flow field to start such a transonic flow simulation from scratch has to be chosen carefully. A direct start with transonic (or supersonic) Mach numbers is not possible because then in all regions even where normally subsonic flow occurs (plenum or most part of the slots) a complete different flow type is initialized compared to final state and lead to heavy gradients in the flow field making convergence problematic. Furthermore, even starting with higher subsonic Mach numbers the nozzle of the wind tunnel will accelerate the initial flow directly to a supersonic wave running through the complete nozzle and destabilizes the flow because of the strong gradients.

The following procedure is instead adopted: first the flow field is initialized with a Mach number around 0.3 (and at the same time adjusting the static pressure and temperature to fit again to the total pressure of

the aimed Mach number). Then after some iterations for stabilization of the flow field, the back pressure on the diffusor outlet is reduced in one or two steps to accelerate the flow in the test section to supersonic speed. After that procedure the flow field can be finally converged down to low error levels.

All free flight simulations started directly at reference Mach number without any additional startup procedure. The reference data in that cases is set on the far field boundary (quadratic box with 100 m size in each direction).

3.0 NUMERICAL RESULTS

In this chapter, the application of the numerical toolchain described above is now demonstrated via a study on wall- and support influences on the WEAG delta wing model. Four different stings with different length and slenderness are evaluated and are compared to the reference: the free flying model without support. The simulations are conducted for both free flight and the in-tunnel situation.

Because especially in transonic and low supersonic Mach number flow sometimes abrupt changes e.g. in aerodynamic coefficients can take place here, a Mach number of Ma = 1.05 is simulated. Furthermore, the model is set at an angle of attack of 20 degree to increase the interaction between sting the model.

3.1 Wall Interference

To identify the effects of wall interference, the cases without a sting are analyzed first. When comparing left versus right in figures 7 and 8, first a slight difference in the oncoming flow Mach number can be identified from free flight (Ma = 1.050) to in-tunnel (Ma = 1.049). This offset of 1 milli-Mach is due to procedure that is followed to set the plenum pressure in the numerical simulation. The plenum pressure was set to the desired test section static pressure which corresponds to the Ma number of 1.05. As the plenum pressure and test section pressure generally differ, a small offset in the Mach number is obtained. This offset can be prevented by conducting a calibration of the empty test section to assess the offset between test section pressure and plenum chamber pressure of the wind tunnel. In the real transonic wind tunnel, this pressure offset is taken into account when setting the plenum pressure and hence, results in the desired Mach number in the test section. In the numerical simulation, this calibration was not incorporated in the procedure.

Table 2: Aerodynamic coefficients of different cases

Case	CL [-]	ΔCL [cts]	CD [-]	ΔCD [cts]	CM [-]	ΔCM [cts]
Free	0.9812	Reference	0.3852	Reference	-0.0595	Reference
Free Slim	0.9834	2.2	0.3770	-82	-0.0592	0.3
Free Standard	0.9836	2.4	0.3769	-83	-0.0592	0.3
Free Short	0.9827	1.5	0.3745	-107	-0.0585	1.0
Free Veryshort	0.9792	-2.0	0.3701	-151	-0.0558	3.7
Tunnel	0.9832	Reference	0.3866	Reference	-0.0602	Reference
Tunnel Slim	0.9868	3.6	0.3786	-80	-0.0599	0.3
Tunnel Standard	0.9866	3.4	0.3784	-82	-0.0600	0.2
Tunnel Short	0.9870	3.8	0.3762	-104	-0.0596	0.6
Tunnel Veryshort	0.9841	0.9	0.3717	-149	-0.0566	3.6

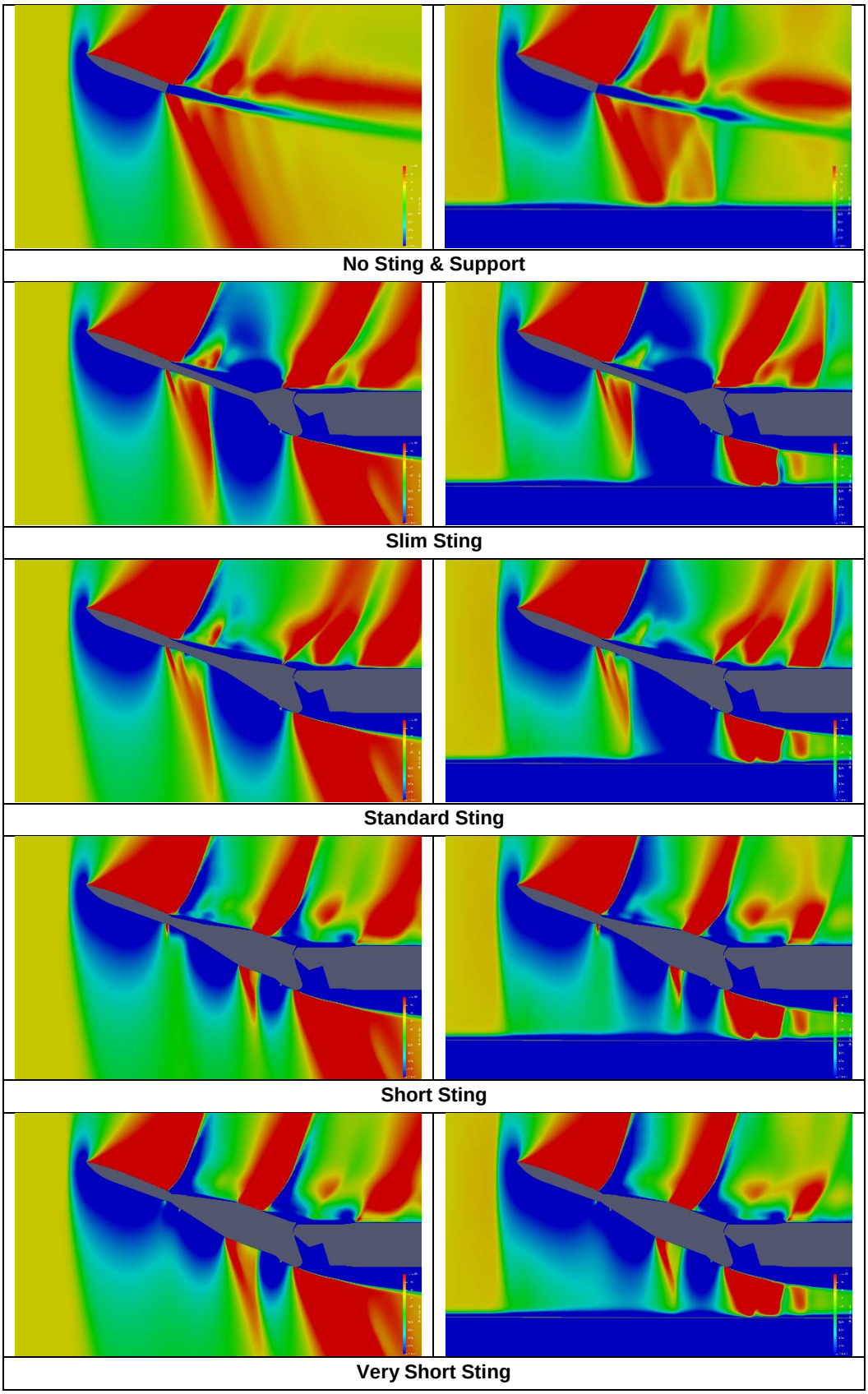

Figure 7: Mach number distributions for free flight (left) and in-tunnel (right) in centreline of the model / tunnel. Mach number from 0.9 (blue) to 1.1 (red).

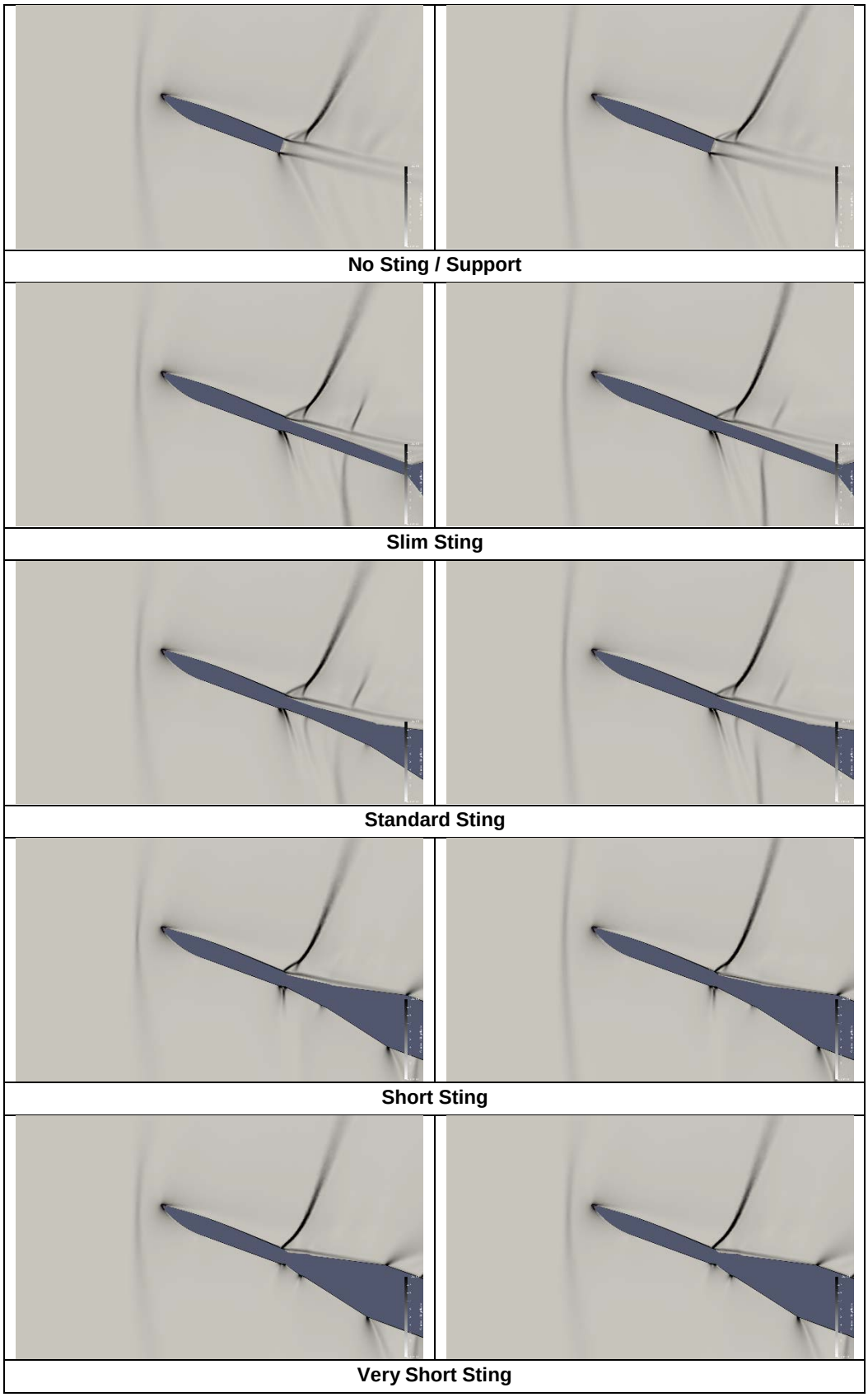

Figure 8: Gradient of density (“Schlieren”) for free flight (left) and in-tunnel (right) in centreline of the model / tunnel

Next, an upstream movement of the bow shock can be identified for the in-tunnel case. (Remark: the in-tunnel pictures cutting the flow field in centerline show a cut through the solid wall between the slots.) Further on, the bow shock is more straight inside the tunnel. Behind the bow shock, the thickness of the boundary layer of the wall (here shown only the lower wall) is increasing due to the pressure rise established by the shock. This thickness gradient changes locally the available cross section of the tunnel stream tube and therefore the linked local Mach number. (Remark: perforated walls do not have such an effect, see chapter 4)

In the region where the expansion wave emanating from the lower trailing edge of the aircraft hits the wall, the thickness of the boundary layer is reduced again because of the local acceleration of the flow and the resulting local pressure reduction.

Comparing the density gradient "Schlieren" from figure 8, one can see that the overall topology of the shocks around the aircraft is unchanged between free flight and the in-tunnel simulation. However, the upstream movement of the bow shock can again be identified.

In Table 2 the aerodynamic coefficients for the different cases are presented. In case of a free flying aircraft, the model sting base cavity is closed and included into the forces and moments integration. This can be directly identified in the drag coefficient, which is lower for all cases with support. The focus in the paper is especially on pitching moment effects although significant drag differences are clearly visible. A comparison in drag with free flying aircraft is difficult to make due to the difference in force integration at the base cavity.

In Table 3 the differences of the pitching moment from free flight to tunnel are presented. The wall influence leads to an additional pitching moment of 0.7 to 1.1 moment count depending on the installed sting. Because no single local change in the flow field around the aircraft is visible with respect to the free flow cases, this is an overall effect summing up small changes because of the tunnel influence.

3.2 Support / Sting Influence

To identify the influence of the sting first, the results for free flight without sting, the slim sting and the standard sting are analysed – compared in either figure 7 or 8. The bow shock and the flow field around the aircraft are unchanged in all three cases. On the lower side of the aircraft, the expansion wave emanating from the lower side of the fuselage trailing edge keeps its upstream position and strength, however further downstream there is a significant change in the local Mach number distribution. The reason is the different effective tunnel cross section and model support interference effects on the wake and flow field. That local change in the boundary condition finally changes the flow field behind the trailing edge shock of the aircraft.

Furthermore, as the cross section of the sting increases towards the main support structure, finally a subsonic pocket is created. In case of the slim sting, the sudden change in cross section leads to a larger area with subsonic flow compared to the standard sting with a more gentle increase in cross section.

Another effect is visible in case of the standard sting. The sting is rotational symmetric – so for an angle of attack of zero, the upper and lower side interact symmetric with the flow. For a 20 degrees angle of attack case, the lower side creates a stronger flow deflection than the upper side and hence, shows a bigger subsonic pocket as the upper side of the sting.

This subsonic pocket created by the support, is the main driver for support interference at transonic Mach numbers. In the three cases discussed, the influence of that subsonic pocket does not reach the final shock front and expansion waves of the aircraft. Hence, the flow field and the resulting pressure distribution of the aircraft is unchanged in these cases. In Table 2 the differences in lift, drag and pitching moment compared to the free flying aircraft are therefore small.

Comparing the flow field (figure 7) for the short sting with the case without sting, the situation now changes on the aircraft: the subsonic pocket is moving upstream into the final shocks of the aircraft and therefore the pressure distribution of the aircraft is locally changed. With regard to pitching moment the difference is now 1.0 count instead of 0.3 in the cases before, the drag increases by 24-25 counts and the lift decreases by 0.7 to 0.9 counts. The subsonic flow field on the lower side of the aircraft is separated from the subsonic pocket upstream of the support by a very small expansion wave at the fuselage trailing edge. In the case of the very short sting both subsonic flow fields unite and the final shock on the upper side of wing is moved even more upstream. Both effects increased the differences to free flight without sting significantly.

The already identified upstream movement of the shocks with increasing sting influence is also visible in the Schlieren pictures (figure 8). Again, for the short and very short sting there is a change in the flow field with the resulting changes in aerodynamic coefficients.

Furthermore, support interference effects are investigated for the in-tunnel cases. Comparing the flow field (figure 7) and the numbers in Table 3, the change in pitching moment with different stings are nearly the same for the free flight and the in-tunnel cases. From this, it is concluded that the wall interference and the support effects at this Mach number can be treated as independent problems at least for a small model like the WEAG. This makes the investigation of support interference effects much easier for numerical simulation because only the free flight cases have to be investigated.

Table 3: Pitching moment coefficient for free flight and in-tunnel

Case	CM Free [-]	CM Tunnel [-]	ΔCM [cts]
Free	-0.0595	-0.0602	0.7
Slim	-0.0592	-0.0599	0.7
Standard	-0.0592	-0.0600	0.8
Short	-0.0585	-0.0596	1.1
Veryshort	-0.0558	-0.0566	0.8

All presented results correspond to a Mach number of 1.05, so very close to the sonic point. The sensitivity of the flow for changes in the (local) cross section and the possibility that even weak shocks lead to subsonic flow, reduces significantly with increasing Mach number. Investigations with the same numerical techniques clearly show that support interference at Ma = 1.2 reduces considerably.

Concluding on the support interference, a proper sting is a compromise between a minimal cross section, mechanical strength, stiffness, stability and length between model and main support system. The current numerical toolchain provides the opportunity to minimize the aerodynamic interferences of the model support system in accordance with the mechanical constraints at high transonic and supersonic conditions. So, the successful design of a sting should include all the presented effects and balance the pros and cons against each other. Overall for the DNW-HST, the available standard sting achieves all these conditions.

4.0 FURTHER INVESTIGATIONS BASED ON NUMERICAL SIMULATION

Besides the example of the support- and wall interference assessment with the WEAG model, the numerical toolchain was further used to investigate effects for bigger models. In that case the sting- and support effects were generally more pronounced; especially at higher angles of attack. By simulations of a given model geometry at different scales, trends were identified for the allowable model size in the trans- and supersonic regime.

At higher angles of attack, it is sometimes necessary to tilt the model reference point above the tunnel centerline to prevent the main support from hitting the lower tunnel wall. Numerical simulations with and without support at different model heights and different x-positions were conducted to identify the effects on the aerodynamic coefficients.

Many polars of different aircraft and in different configurations (e.g. flap settings) were investigated at Mach number of 1.05, as well as higher Mach numbers like 1.20 and 1.25. At these conditions, the assessment of changes in support- and wall interference was of main interest here. The numerical simulation was further used to better understand the slot flow behaviour, the effect of additional side wall ventilation and changes in the slot geometry itself. Another working field was the detailed analysis of the effects of the re-entry settings of the tunnel.

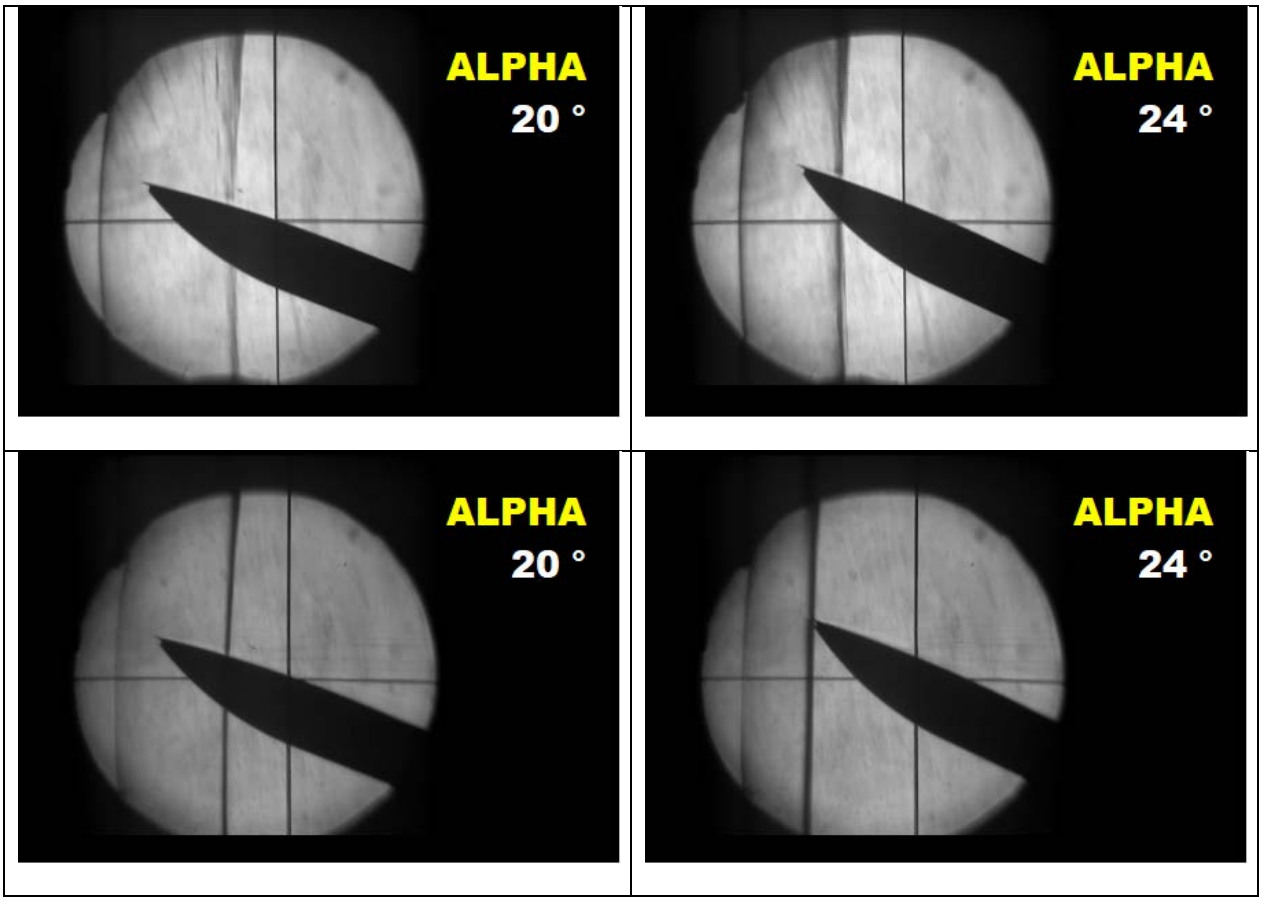

Figure 9: Measured Schlieren results at Ma=1.10.
Upper is perforated walls. Lower is slotted walls.

Regarding the tunnel operation, the regulation of the plenum pressure by an active suction system in the plenum instead of the passive system with the existing re-entry system was investigated and weighted against the additional complexity and cost of such an active suction system. For these investigations multiple variation of slat and flap of the re-entry system were considered, along with variation in the axial cross-section area distribution of the diffusor. The aim of these studies was to optimize the tunnel operation range in terms of Mach number and angle of attack while at the same time trying to minimize the power consumption.

The control of the terminating shock turns out to be a key element of the power optimization. It was found by reducing the back pressure that at some point, the terminating shock can move further down in the diffusor (depending on the slat/flap setting) increasing at the same time the power losses there and the

(passive) control on the plenum pressure is lost because no subsonic connection between plenum and diffusor exists anymore. Keeping the terminating shock on the trailing edge of the slats is therefore the aim of slat/flap setting optimization.

Finally, it was found that when testing models in the slotted test section at transonic Mach numbers close to unity (e.g. Ma = 1.05), it is hard to maintain the same wall boundary layer characteristics as during the empty test section calibration. The incoming model shocks interact with the wall boundary layer which generally causes a notable thickening and thereby a reduction in the tunnel cross-section and hence the local supersonic Mach number.

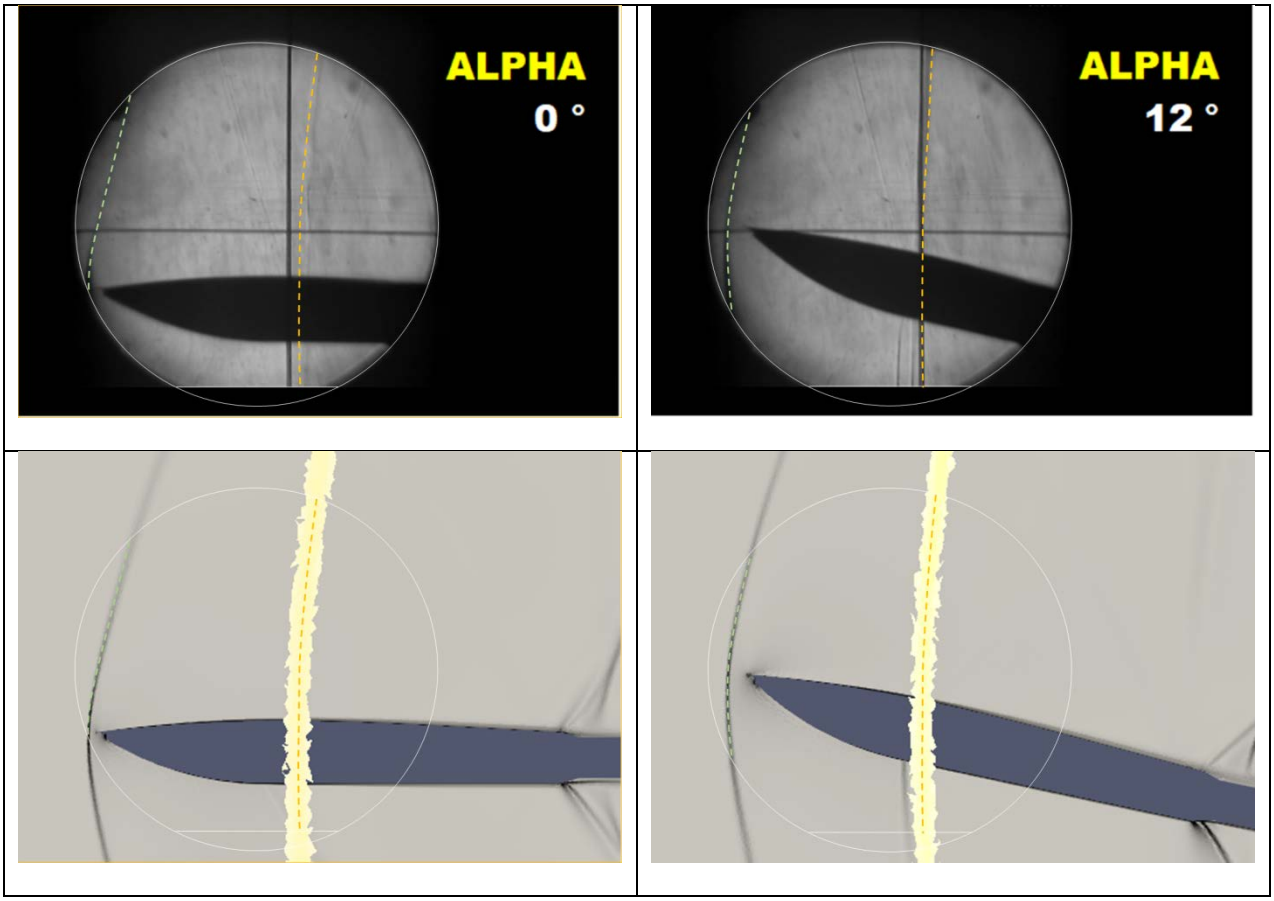

Figure 10: Measured Schlieren and computed density gradient results at Ma=1.10. Upper is measured in the slotted HST. Lower is computed for the slotted HST at tunnel center. White lines mark the Schlieren observation window in the experiment. Yellow band represents the computed bow shock location close to the sidewalls. Dashed green line is the bow shock at tunnel center, dashed orange line is the bow shock close to the sidewalls both from measurement.

To move away from this inherent drawback of slotted walls, additional numerical simulations of perforated walls were undertaken (with all holes fully resolved by numerical simulation). These studies showed that perforated walls, especially ones with slanted holes, have more favourable wave cancelation properties than the slotted walls have. The improved wave cancelation characteristics improves the consistency of the local Mach number distribution around the model, even at higher angles of attack. These initial simulations of perforated walls quickly led to further studies for the effects of parameters such as opening ratio, distribution of the holes and the transition from the closed wall in the Laval nozzle to the ventilated test section itself. The numerical toolchain proved to be a valuable tool for identifying the various trends.

The results of the studies finally drove the decision in early 2020, to design and produce an additional set of perforated walls for the DNW-HST. The wind tunnel can now be configured with either slotted or perforated walls. The first results of back-to-back testing of the physical WEAG TA-15 model in each test section are shown in figure 9. The Schlieren from the perforated test section reveals a more oblique bow shock in front of the model compared to the slotted test section. In the perforated test section, the bow shock is also found to reflect in the Schlieren window at a further downstream location than for slotted.

For the WEAG TA-15 model, further on comparisons from experiment in slotted walls with the equivalent numerical simulation results can be found in figure 10. The computed density gradients for the slotted CFD wind tunnel reveal a bow-shock and reflection wave pattern that matches well with the measured Schlieren in the real HST. The computed free-flight solutions have been omitted here to avoid confusion as the point where the bow-shock impinges on the hard Schlieren window will always occur at a more upstream position in-tunnel as it does in free flight. This is because in free flight the flow is not required to continuing parallel to a wall across the shock. Overall, the comparison of the real and numerical wind tunnel results are similar, which is an example of the strength of the complementary use of numerical simulation for wind tunnel test analysis and for redesign of wind tunnel components.

5.0 CONCLUSION AND FURTHER WORK

The aim of this paper was to develop, implement and demonstrate a numerical simulation strategy to increase the understanding of the wind tunnel environment at trans- and supersonic Mach numbers. This formed the basis for an optimization of the DNW-HST regarding flow quality, power consumption, Mach number range and some non-linearities taking place e.g. with bigger models in the test section. A large number of model and tunnel configurations were therefore investigated numerically.

As an example, numerical simulation results for a basic delta wing configuration (WEAG TA-15) were presented for the free flight and the in-tunnel environment including the slotted walls at identical reference flow conditions at transonic Mach number of 1.05. In both environments, the model without support and model with four different model supports were simulated to establish the interference of the empty test section, the model support system and the wall-test article interactions. The benefit of using numerical simulation is that it offers the possibility to provide more consistent results for both environments – which is much more complex or even not possible in an experimental approach.

This paper demonstrates that the analysis of transonic flow fields based on numerical simulation is ready for analysis of transonic wind tunnel problems and (re-)design of new tunnels, or tunnel components. These numerical simulations can now be used to identify trends and answer tunnel design questions – as well as bring benefits in terms of the analyses and interpretation of actual experimental results.

The demonstrated combination of numerical simulation and experiment lead to significant improvements for the DNW-HST. The main results are the implementation of a set of perforated walls in the year 2020 to improve the flow quality at transonic and low supersonic Mach numbers. Furthermore, at the same time, the re-entry system was optimized driven by CFD results to improve the Mach number range for bigger models and at the same time minimize the power consumption.

REFERENCES

[1] Chwalowski, P.; Silva, W.A.; Wieseman, C.D.; Heeg, J.: "CFD Model of The Transonic Dynamics Tunnel with Applications.", Paper 09, NATO STO-MP-AVT-284, 2018.

[2] Crippa, S., "Improvement of Unstructured Computational Fluid Dynamics Simulations Through Novel Mesh Generation Methodologies" Journal of Aircraft 3/48, pp. 1036-1044, 2012.

[3] Eisfeld, B., Rumsey, C., Togiti, V.: "Verification and Validation of a Second-Moment-Closure Model.", AIAA Journal, Vol. 54 No. 5 (2016) 1524-1541, 2016.

[4] Eisfeld, B., Rumsey, C.L.: "Length-Scale Correction for Reynolds-Stress Modelling.", AIAA Journal, Vol. 58 No. 4 (2020) 1518-1528, 2020

[5] Gebbink, R.; Kapteijn, K.; Bai, F.; Mao, K., Zhang, D.; Ba, Y., Zhang, M.: "Consistency Verifications of the DNW-HST Tunnel Interference Correction Bookkeeping.", AIAA 2018-2116, AIAA Aerospace Sciences Meeting, Kissimmee, Florida, 2018.

[6] Glazkov, S. A.; Gorbushin, A.; Ivanov, A.; Semenov, A.; Vlasenko, V.; Quest, J.: "Numerical and Experimental Investigations of Slot Flow with Respect to Wind Tunnel Interference Assessment.", AIAA Paper 2004-2308, 2004

[7] Goffert, B.; Ortega, M.A.; Filho J.B.P.F.: "Numerical Study of Wall Ventilation in a Transonic Wind Tunnel," Journal of Aerospace Technology and Management, vol. 7, pp. 81-92, 2015.

[8] Hashimoto, A.; Kohzai, M.: "Wall Interference Analysis by Whole Wind Tunnel CFD," in 5th Symposium on Integrating CFD and Experiments in Aerodynamics, 2012.

[9] Hantrais-Gervois, J.-L.; Piat, J.-F.: "A Methodology to Derive Wind Tunnel Wall Corrections from RANS Simulations", Paper 14, NATO STO-MP-AVT-284, 2018.

[10] Koenig, B.; Fares, E.; Wright, M.C.N.: "Lattice Boltzmann Simulation of the ETW Slotted Wall Test Section", Paper 12, NATO STO-MP-AVT-284, 2018.

[11] Kursakov, I.A.; Gorbushin, A.R.; Bosnyakov, S.M.; Glazkov, S.A.; Lysenkov, A.V.; Matyash, S.V.; Semenov, A.V.; Quest, J.: "A numerical approach for assessing slotted wall interference using the CRM model at ETW," CEAS Aeronautical Journal, p. 1-20, 2017.

[12] Leatham, M. and Stokes, S. and Shaw, J. A. and Cooper, J. and Appa, J. and Blaylock, T., "Automatic Mesh Generation for Rapid-Response Navier-Stokes Calculations" AIAA 2000-2247, FLUIDS 2000 Conference and Exhibit, June 2000, 2000.

[13] Maseland, J.E.J.; Laban, M.; Ven, H.; Kooi, J.W.: "Development of CFD-based interference models for the DNW-HST transonic wind tunnel," National Aerospace Laboratory NLR, NLR-TP-2006-504, 2006.

[14] Melber-Wilkending, S.; Wichmann, G.: "Application of Advanced CFD Tools for High Reynolds Number Testing," in 47th AIAA Aerospace Sciences Meeting, AIAA 2009-418, 2009.

[15] Olander, M.: "CFD Simulation of the Volvo Cars Slotted Walls Wind Tunnel.", Chalmers university of technology, Goteborg, Sweden, 2011.

[16] Rivers, S.M.; Nayani, S.N.; Tinetti, A.F.; Brynildsen, S.E.; Ferris, R.J.: "Numerical Study of the High-Speed Leg of the National Transonic Facility", Paper 13, NATO STO-MP-AVT-284, 2018.

[17] Rivers, M.; Dittberner, A.: "Experimental Investigations of the NASA Common Research Model in the NASA Langley National Transonic Facility and NASA Ames 11-Ft Transonic Wind Tunnel.", Paper 06, NATO STO-MP-AVT-284, 2018.

[18] Schuman, W.C.: "A Computational Evaluation of Transonic Wind Tunnel Wall Interference on High Aspect Ratio Models in the Arnold Engineering Development Complex 16 Foot Transonic Tunnel.,"University of Tennessee, 2016.

[19] Schwamborn, Dieter and Gerhold, Thomas and Heinrich, Ralf, “The DLR TAU-Code: Recent Applications in Research and Industry”, ECCOMAS CFD, P. Wesseling, E. O.J. Periaux (Eds), TU Delft, The Netherlands, 2006.

[20] Spalart, P. R., and Allmaras, S. R., "A One-Equation Turbulence Model for Aerodynamic Flows," AIAA Paper 1992-0439, 1992.

[21] Wubben, F.; Maseland, H.: "Verification of wind tunnel model support and wall interference assessments in DNW-HST by CFD simulations", Paper 05, NATO STO-MP-AVT-284, 2018.

[22] Wubben, F.; Takara, E.: "Wind tunnel model support and wall interference corrections in DNW-HST - ensuring high data quality standards.", 5th CEAS Air & Space conference, 2015.